Graphene Oxide of Extra High Oxidation: A Wafer for Loading Guest Molecules

Abdelsattar O. E. Abdelhalim[a,b], Vladimir V. Sharoyko[a,c,d], Sergei V. Ageev[c,a], Vladimir S. Farafonov[e], Dmitry A. Nerukh[f], Viktor N. Postnov[a], Andrey V. Petrov[a], Konstantin N. Semenov[c,a,d*]*

[a]Institute of Chemistry, Saint Petersburg State University, 26 Universitetskii prospekt, Saint Petersburg, 198504, Russia

[b]Environmental Research Department, National Center for Social and Criminological Research (NCSCR), Giza 11561, Egypt

[c]Pavlov First Saint Petersburg State Medical University, 6–8 L'va Tolstogo ulitsa, Saint Petersburg, 197022, Russia

[d]A. M. Granov Russian Research Centre for Radiology and Surgical Technologies, 70 Leningradskaya ulitsa, Saint Petersburg, 197758, Russia

[e]V. N. Karazin Kharkiv National University, 4 Svobody ploshchad', Kharkiv, 61022, Ukraine

[f]Department of Mathematics, Aston University, Birmingham, B4 7ET, The United Kingdom

[*]Corresponding authors at: 6–8 L'va Tolstogo ulitsa, Saint Petersburg, 197022, Russia (K. N. Semenov) and 26 Universitetskii prospekt, Saint Petersburg, 198504, Russia (V. V. Sharoyko). E-mail addresses: knsemenov@gmail.com (K. N. Semenov), sharoyko@gmail.com (V. V. Sharoyko).

1   **Abstract**

2   We present a new modification of graphene oxide with very high content (85 wt. %) of

3   oxygen-containing functional groups (hydroxy, epoxy, lactol, carboxyl, and carbonyl groups) that

4   forms stable aqueous dispersion in up to 9 g·l^{-1} concentration solutions. A novel faster method of

5   the synthesis is described that produces up to 1 kg of the material and allows controlling the particle

6   size in solution. The synthesised compound was characterised by various physicochemical

7   methods and molecular dynamics modelling revealing unique structure in the form of multi-

8   layered wafer of several sheets thick, where each sheet is highly corrugated. The ragged structure

9   of the sheets forms pockets with hindered mobility of water that leads to the possibility of trapping

10   guest molecules.

85 wt. % oxidation

Wafer structure

11

12
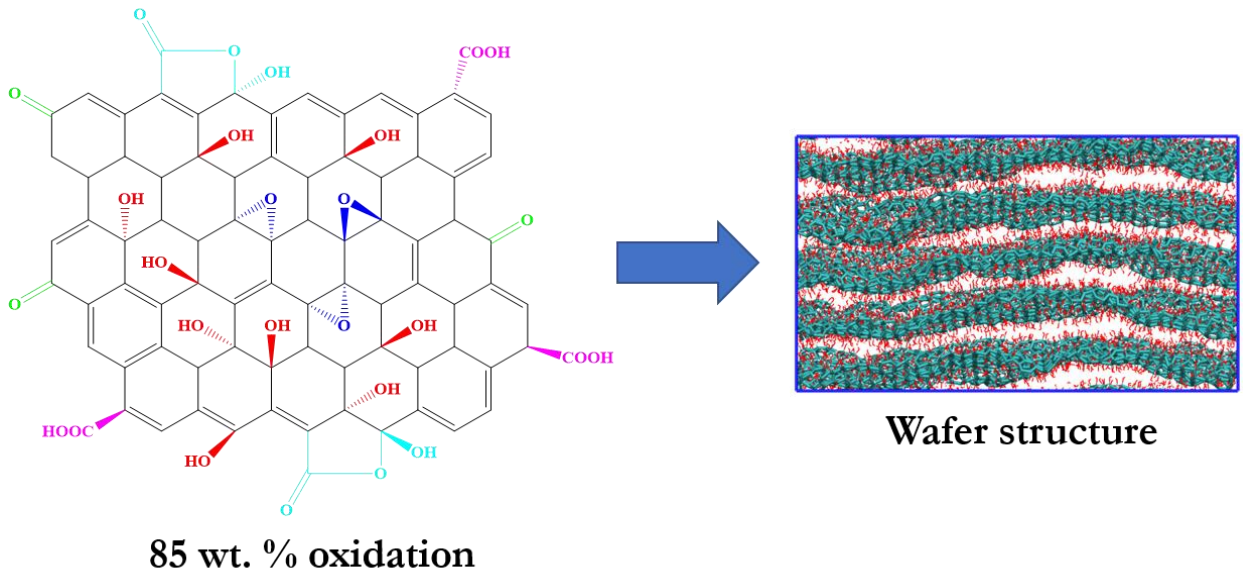
2

1   Unique thermal, chemical, mechanical, electronic, electrical and optical properties of

2   graphene and its oxidised form graphene oxide (GO) [1–9] determine their applications in energy

3   (solar cells, batteries, supercapacitors, fuel cells [10–17]), electronics [18–20], optics [21], sensor design

4   [14,22,23], textiles [24], water disinfection [25–27] and desalination [28,29], as well as in biomedical areas such

5   as targeted drug [30,31] and biomolecule [32–38] delivery, tissue engineering [39], diagnostics [40–42] and

6   bioimaging [43–46], photodamage protection [47], development of nanomaterials with antiviral [48],

7   antibacterial [49], antifungal [50], and anticancer activity [51–53]. When discovered in 2004 by Geim and

8   Novoselov, graphene was obtained through a simple mechanical method by separating one layer

9   from graphite material [54]. To date, various methods of graphene synthesis were designed including

10   chemical vapour deposition [55], electrochemical exfoliation of graphite [56], mechanical exfoliation

11   [57], and reduction of GO thermally [58], chemically [59] or electrochemically [60].

12   GO is an oxidised form of graphene that contains oxygen functional groups, such as

13   carbonyl, carboxyl, and lactol groups at the edges of GO flakes as well as hydroxyl and epoxy

14   groups located at the basal plane of the flake surface. Oxidising graphene surface brings several

15   physical, chemical, and biological advantages, specifically, (*i*) the ability to form a stable

16   dispersion due to the interaction of the oxygen functional groups with water molecules through

17   hydrogen bonds; (*ii*) the possibility of further functionalisation exploiting various functional

18   groups located on the GO surface.

19   Interestingly, GO was synthesised before graphene, first by Brodie in 1859 [61] from graphite

20   using potassium chlorate and fuming nitric acid as the oxidising agents and then by Staudenmaier

21   in 1898 [62] with some modifications for the oxidation method using potassium chlorate,

22   concentrated sulphuric acid, and fuming nitric acid. In 1937, Hofmann utilised non-fuming nitric

23   acid with potassium chlorate [63]. Hummers and Offeman in 1958 synthesised GO by oxidising

graphite using a mixture of oxidising agents: sulphuric acid, sodium nitrate, and potassium permanganate. The method was called Hummers' method [64]. In 2010, Tour developed a modification of the Hummers' method by replacing sodium nitrate with phosphoric acid for improved oxidation and using H_2SO_4 / H_3PO_4 mixture with the 9:1 ratio [65]. Currently Hummers' method and its modifications, and Tour's method are usually used for obtaining GO, rather than Brodie's and Staudenmaier's methods, as faster and safer methods [66]. An additional advantage is higher oxygen content in Hummers' (52.89 %) and Tour's (55.86 %) methods comparing to Hofmann's (45.50 %) and Staudenmaier's (44.89 %) methods.

Graphene and its derivatives are intensively studied using computational methods [67–73]. In particular, molecular dynamics (MD) modelling of graphene oxide was utilised to investigate the molecular details of GO, including its interaction with water, its aggregation properties, physicochemical and mechanical characteristics [74–79].

Here we present a new modification of GO with even higher content of oxygen-containing functional groups (up to 85 wt. %). We describe a new method of synthesis as well as physicochemical characterisation of the material using experimental and computational methods. We show that this new GO compound has unique structure that is capable of trapping a variety of guest molecules not only as chemical conjugates but also between the sheets in formed pockets filled with immobilised water.

The proposed method of synthesis has the following advantages over the analogues: (*i*) increased, up to 95 %, yield of the product due to the new ratio between the reagents ($KMnO_4$ and graphite, graphite and H_2SO_4, H_2SO_4 and H_2O, H_2SO_4 and H_2O_2); (*ii*) increased content of the oxygen-containing functional groups (carboxyl, carbonyl, hydroxyl, epoxy, lactol) due to the use of additional oxidants, with the oxidiser ($NaNO_3$, P_4O_{10}) weight ratio of 10 (graphite) to 1

1 (oxidiser); (*iii*) the ability to obtain stable aqueous dispersions of GO without adding surfactants;

2 (*iv*) the reduced time of synthesis (4 h); (*v*) the ability to control the size of the resulting

3 nanoparticles due to an additional stage with temperature treatment of the reaction mixture at 95°C;

4 (*vi*) scaling of the GO production process up to 1 kg.

5   For GO synthesis, the graphite powder was used having the following characteristics:

6 particle size <45 μm, 99.99 % purity. In a round-bottom flask 500 g of graphite, 50 g of P_4O_{10}, and

7 2.5 l of H_2SO_4 were mixed and treated in an ultrasonic bath ODA-DS40, Russia (ultrasonic

8 frequency 37 kHz, ultrasonic power 160 W) for 10 min, then the resulting mixture was stirred for

9 15 min at room temperature. Thereafter, 50 g of $NaNO_3$ was gradually added to the reaction

10 mixture while cooling on ice to 5°C with continuous stirring for 30 minutes. Next, 500 g of $KMnO_4$

11 were added with continuous stirring for 30 min (the temperature was maintained at 5 °C using ice),

12 and then the temperature was increased to 40°C for 1 h with continuous stirring, followed by the

13 gradual addition of 1.25 l of distilled water. After that, the temperature of the reaction mixture was

14 increased to 95°C for 1.5 h, then 2.5 l of distilled water and 50 ml of 30 % H_2O_2 were added. The

15 resulting precipitate was separated from the solution using a Schott filter (pore size 1.6–4.0 μm),

16 washed with 5 % HCl, then distilled water was added until neutral pH, dried at 65°C, and dissolved

17 in distilled water in an ultrasonic bath for 1 h for exfoliation.

18   The obtained dispersions of GO in the concentration range $C = 1.8–9.0$ g·l^{-1} are shown in

19 Fig. 1 in comparison with distilled water. Even the solution of highest concentration forms a stable

20 transparent dispersion for more than one month.

21   Fig. 2 shows the ^{13}C NMR spectrum obtained by direct excitation. The spectrum reveals

22 the following peaks: (*i*) the weakly pronounced peak at 60 ppm corresponding to the epoxy groups;

23 (*ii*) the intense peak at 69 ppm attributed to the hydroxyl groups; (*iii*) the low-intensity peak at 100

ppm corresponding to the carbon atom in the lactol group; (*iv*) the peak at 129 ppm attributed to the C=C structural fragment of the graphene plane; (*v*) the weak peak at 165 ppm corresponding to the carboxyl groups; (*vi*) the broad peak at 191 ppm corresponding to the carbonyl groups. From these data, the percentage of the oxygen-containing functional groups on the surface of GO was determined to be 55 85 wt. % for hydroxyl groups, 22 wt. % for epoxy groups, 4 wt. % for lactol groups, 3 wt. % for carbonyl groups, 1 wt. % for carboxyl groups (85 wt. % in total), which was consistent with available experimental data [80–84].

The IR spectrum of GO is presented in Fig. 3*a*. The broad peak at 3440 cm^{-1} refers to the stretching of the O–H fragment of the hydroxyl, carboxyl and lactol groups; the intense peak at 1718 cm^{-1} corresponds to the stretching of the C=O fragment of the carboxyl, carbonyl and lactol groups; the three peaks at 1363, 1418 and 1226 cm^{-1} refer to the stretching of the C–OH fragment of the hydroxyl groups from the hydroxyl, lactol and carboxyl groups respectively, the peak at 1085 cm^{-1} corresponds to the stretching of C–O in the epoxy groups; the peak at 1630 cm^{-1} corresponds to the stretching of graphene C=C aromatic domains. The obtained results are in agreement with the literature data [85,86].

Fig. 3*b* demonstrates the UV/Vis spectrum of GO in the wavelength range λ = 200–800 nm. The absorption peak at 235 nm corresponds to π–π* transitions of the remaining sp^2 C=C bonds of GO. The shoulder at 300 nm is related to the n–π* transitions of C=O bonds of the carboxyl, carbonyl and lactol groups. The obtained spectrum is in good agreement with the literature data [87,88].

Fig. 3*c* shows the results of Raman spectroscopy of a GO sample. The spectrum contains D, G and 2D bands. The G band is characteristic of all sp^2-hybridised graphite-like materials; it shows that the synthesised sample contains a C=C fragment that forms a π-structure. The D band

1 describes a defect mode associated with the functionalisation of the surface, leading to the

2 transition of carbon atoms to the sp^3-hybridised state and disordering the π-system. The 2D band

3 describes the number of graphene layers and determines whether these structures are single-

4 layered, double-layered, or multi-layered. In particular, in the case of single-layer GO, the ratio

5 I_{2D} / I_G is equal to 2; a decrease in this ratio indicates an increase in the number of layers. The $I_D /$

6 I_G ratio allows to estimate the degree of functionalisation of the GO surface as well as the defect

7 content. The analysis of Fig. 3c shows the presence of D and G bands at 1360 cm^{-1} and 1592 cm^{-1},

8 having the I_D / I_G ratio of 0.97, indicating the functionalisation of the graphene surface with oxygen

9 functional groups confirming the formation of GO. The analysis of Raman spectrum shows

10 agreement with the literature results [89–94].

11 In summary, the applied techniques provide consistent picture for the chemical structure

12 of the synthesised compound with very high quantity of oxygen containing groups and specific

13 distribution between various groups that we used in our subsequent MD simulations.

14 The presence of the 2D band (ratio I_{2D} / I_G = 0.65) in Raman spectrum indicates a multi-

15 layered structure of GO. We now concentrate on determining the properties of this wafer-like

16 structure.

17 The analysis of graphite and GO X-ray diffraction spectra (see the spectra in Appendix 1)

18 shows that the peak of the 002 plane of graphite was found at $2\theta = 26.5°$, while after oxidation the

19 peak shifted to $2\theta = 9.68°$ representing the 001 plane of GO. This fact confirms the oxidation of

20 graphite to GO. To estimate the inter-molecular distance between the GO sheets, Bragg's law was

21 applied [95]:

22 $\lambda = 2d \sin\theta$ (1),

where λ is the wavelength of the X-ray beam (0.154 nm), d is the distance between the adjacent GO sheets or layers, θ is the diffraction angle. The diffraction peak was at $2\theta = 9.68°$, representing the (001) planes, the spacing between which was the distance between the GO sheets which, in our case, was equal to 9.13 Å (the value in literature is in the range 6–11 Å [78]). This particular value is explained by a unique structure of the layer, the details are revealed by MD simulation, see below.

Fig. 4 shows SEM and HRTEM images of GO. It can be seen that the synthesised sample consists of delaminated crumpled layers with sharp edges. At the same time, HRTEM analysis shows that the structure of GO consists of smooth transparent flakes with organised distribution and homogeneous surface without agglomerations. The number of layers is low, even bilayers and single layers of GO sheets are visible with twisted or wrinkled edges due to functionalisation and different interactions between the functional groups on the surface. This leads to the high density of functional groups on the surface that help increase the distance between the layers to account for transparency and preventing the accumulation of the layers.

When dissolved in water, the flakes form associates. The dynamic light scattering analysis of the obtained size distribution reveals that the average size of GO associates is 300–350 nm. At the same time, the values of ζ-potentials ($-(35-30)$ mV) prove that the obtained dispersions possess aggregative stability (see Fig. 3 in the Appendix 1) [96].

The obtained adsorption isotherm is presented in Fig. 5. According to the BET classification, this isotherm can be attributed to type B. Such isotherms are observed in the case of the adsorption on layered structures, in particular, the adsorption of non-polar vapours on montmorillonite [97]. When interpreting such isotherms, it is assumed that such form of a desorption branch is due to the evaporation of the adsorbate between plate-shaped particles, which are

1   oriented by the surface tension forces into a thixotropic structure. During desorption, the amount

2   of capillary condensate decreases and the thixotropic structure is disordered. Rapid evaporation of

3   the adsorbate leads to the formation of a step in the desorption curve. The surface was determined

4   by the DFT method and corresponds to (26.6 ± 2.6) m$^2 \cdot$g^{-1}. Usually, the GO surface area according

5   to the literature data is estimated to be 200–600 m$^2 \cdot$g^{-1} [98,99], and the low surface area is due to the

6   association of the layers *via* hydrogen bonds. Similar results were previously obtained by Ding *et*

7   *al.* [100] for GO obtained from the waste graphite from diamond synthesis industry.

8   In summary, experimental data show that the synthesised GO sheets form multi-layers

9   structures, of few sheets thick, that are flexible and associated into several hundred nanometres

10   large particles when dissolved in water. The structures are capable of absorbing nitrogen in a

11   manner characteristic to inter-layer absorption/desorption process.

12   In order to elucidate the spatial structure of the material and explain its unique properties

13   in hosting molecules we have performed MD modelling closely mimicking the realistic GO with

14   chemical and physical properties revealed by the experiment.

15   The models of GO sheets were prepared in several stages. First, a flat 8×8 nm square

16   graphene sheet (2,508 atoms) was generated using the VMD Nanotube builder plugin [101]. Then,

17   the hydroxyl and epoxy groups were attached to randomly chosen carbon atoms from both sides.

18   The correctness of the produced structure was checked in terms of the absence of tri- or pentavalent

19   carbon atoms. Five GO sheets with unique distributions of groups were prepared by this procedure.

20   The size of real sheets is in hundreds of nanometres or even micrometres that far outreaches

21   the conventional targets of MD. Therefore, we used periodic boundary conditions to mimic sheets

22   that are "infinitely large" from the microscopic point of view. For this, in the atomistic models the

23   atoms located at any sheet edge were made matching those located at the opposite edge.

The number of groups of each kind corresponded to their experimentally measured content. According to the NMR results (Fig. 2), carbon atoms are functionalised with 55 wt. % hydroxyl groups, 22 wt. % epoxy groups, as well as with 8 wt. % groups, which can be situated only at edges. Consequently, among the subset of non-edge carbon atoms, the fractions of atoms bound to hydroxyl and epoxy groups are (100/92) ~ 1.09 times higher than the overall values, resulting in 60 wt. % and 24 wt. %, respectively. Because we modelled the "edge-less" sheets, we employed the latter percentages in our atomistic models.

The details on the forcefield and other specifics of the MD setup are provided in Appendix 2.

We simulated two kinds of systems: a single GO sheet in water and a stack of five sheets in water, Fig. 6. For the latter systems, eight configurations were prepared. Configurations #1–#3 were made by placing the sheets in empty box at different inter-sheet spacing with subsequent solvation and energy minimisation. The values 0.75, 1.15, 1.5 nm were taken, where the former two values correspond to a single or double layer of water molecules fitted between the sheets [79]. In contrast, in configuration #4 the sheets were placed with 1.5 nm spacing and then simulated in vacuum for 10 ns. At such conditions the sheets were allowed to approach each other as close as possible. The resulting configuration having variable spacing was then solvated and used as the initial structure, Fig. 6*d*. Configurations #5–#8 were made exactly in the same way as #1–#4 but had two non-adjacent sheets initially mirrored with respect to their basal planes. The details of the prepared GO stacks are listed in Table 1.

The single GO sheet, which was flat in the initial configuration, was considerably deformed and adopted a strongly rugged shape during the first picoseconds of MD. This shape stayed conserved afterwards, and no further deformations or fluctuations occurred, Fig. 7*a*. The

magnitude of roughness, estimated as the distance between the points located farthest out of plane at each side, reached 1.2 nm. This finding seems somewhat surprising, as we have found no evidence for observing such non-flat GO structures in the available literature. However, it can readily be explained by the vast prevalence of sp^3-hybridised carbon atoms tending to adopt a tetrahedral coordination and the strong repulsion between closely packed oxygen atoms.

The stacks of five sheets behaved in similar fashion, Fig. 7*bc*. Each sheet was deformed to the thickness of 1.2–1.4 nm in all cases. The original spacing has considerably changed from the initial value in response to the deformation of the sheets. Its average final value was calculated by dividing the cell thickness by the number of sheets (that is five), Table 1. As a result, the contact between the sheets appeared rather loose and occurring not across the whole plane, but only at some regions.

The results indicate that the shortest average distance between sheets that can be achieved is ~0.9 nm. This is much thicker than for the less functionalised GO, where 0.6 nm is possible if no water layer is present [79]. The reason is the highly rough shape of the sheets that prevents tight packing. This fact also allows numerous water molecules to be placed in the gaps between adjacent sheets, which however form not a continuous layer but a set of weakly connected basins, Fig. 7*d*.

The similarity of final thicknesses between stacks #1 and #4, #2 and #5 etc. indicates that the values are robust and do not substantially depend on the functionalisation patterns of the sheets taken for simulation.

Considering the dynamics of the simulated systems, the lateral motion of the sheets in all stacks was strongly hindered because the adjacent sheets formed contacts. The mobility of water molecules was reduced, as well, due to the hydrogen bonding with GO. We estimated the diffusion coefficient D of water over the MD trajectories. For most stacks D is less than $0.05 \cdot 10^{-9}$ m$^2 \cdot$s^{-1}

indicating that it is almost completely bound to GO. Only in the stacks #3 and #5 with the largest spacing and highest content of water $D = 0.2 \cdot 10^{-9}$ m$^2 \cdot$s^{-1} that is somewhat higher. For comparison, the bulk value for SPC/E water is $2.7 \cdot 10^{-9}$ m$^2 \cdot$s^{-1} [102].

Summarising, for the first time, the express synthesis method was developed leading to the formation of GO enriched with oxygen-containing functional groups up to 85 wt. % (hydroxyl (55 wt. %), epoxy (22 wt. %), lactol (4 wt. %), carbonyl (3 wt. %), and carboxyl (1 wt. %) groups). The proposed technique has several advantages including the high yield of the product (95 %), the reduced time of synthesis (4 h), scaling up the GO production (1 kg), the diverse possibilities of further chemical modification, the formation of stable aqueous dispersions. The obtained material was characterised with a set of physicochemical techniques as well as simulated using MD, which reveal that it has multi-layered structure of several sheets thick, where each sheet is highly corrugated. The sheets form associates that in solution produce stable dispersions even at high concentration with particle size of several hundred nanometres. The unique ragged structure of the sheets forms pockets with hindered mobility of water that leads to the possibility of trapping guest molecules.

5   **Supporting Information Available**: Description of the material included.

6

References

(1)   Falkovsky, L. A. Optical Properties of Graphene and IV–VI Semiconductors. *Physics-Uspekhi* **2008**, *51*, 887–897.

(2)   Hussain, S.; Iqbal, M. W.; Park, J.; Ahmad, M.; Singh, J.; Eom, J.; Jung, J. Physical and Electrical Properties of Graphene Grown under Different Hydrogen Flow in Low Pressure Chemical Vapor Deposition. *Nanoscale Res. Lett.* **2014**, *9*, 546.

(3)   Shahil, K. M. F.; Balandin, A. A. Thermal Properties of Graphene and Multilayer Graphene: Applications in Thermal Interface Materials. *Solid State Commun.* **2012**, *152*, 1331–1340.

(4)   Mao, H. Y.; Lu, Y. H.; Lin, J. D.; Zhong, S.; Wee, A. T. S.; Chen, W. Manipulating the Electronic and Chemical Properties of Graphene *via* Molecular Functionalization. *Prog. Surf. Sci.* **2013**, *88*, 132–159.

(5)   Papageorgiou, D. G.; Kinloch, I. A.; Young, R. J. Mechanical Properties of Graphene and Graphene-Based Nanocomposites. *Prog. Mater. Sci.* **2017**, *90*, 75–127.

(6)   Novoselov, K. S.; Morozov, S. V.; Mohinddin, T. M. G.; Ponomarenko, L. A.; Elias, D. C.; Yang, R.; Barbolina, I. I.; Blake, P.; Booth, T. J.; Jiang, D.; *et al.* Electronic Properties of Graphene. *Phys. status solidi* **2007**, *244*, 4106–4111.

(7)   Kumar, P. V.; Grossman, J. C. *Enhanced Electrical, Optical and Chemical Properties of Graphene Oxide through a Novel Phase Transformation*; Massachusetts Institute of Technology: Cambridge, USA, 2015.

(8)   Zhu, Y.; Murali, S.; Cai, W.; Li, X.; Suk, J. W.; Potts, J. R.; Ruoff, R. S. Graphene and Graphene Oxide: Synthesis, Properties, and Applications. *Adv. Mater.* **2010**, *22*, 3906–3924.

(9)   Poklonski, N. A.; Vyrko, S. A.; Siahlo, A. I.; Poklonskaya, O. N.; Ratkevich, S. V; Hieu,

N. N.; Kocherzhenko, A. A. Synergy of Physical Properties of Low-Dimensional Carbon-Based Systems for Nanoscale Device Design. *Mater. Res. Express* **2019**, *6*, 042002.

(10) Chen, D.; Zhang, H.; Liu, Y.; Li, J. Graphene and Its Derivatives for the Development of Solar Cells, Photoelectrochemical, and Photocatalytic Applications. *Energy Environ. Sci.* **2013**, *6*, 1362–1387.

(11) Zhang, C.; Mahmood, N.; Yin, H.; Liu, F.; Hou, Y. Synthesis of Phosphorus-Doped Graphene and Its Multifunctional Applications for Oxygen Reduction Reaction and Lithium Ion Batteries. *Adv. Mater.* **2013**, *25*, 4932–4937.

(12) Yang, Z.; Chabi, S.; Xia, Y.; Zhu, Y. Preparation of 3D Graphene-Based Architectures and Their Applications in Supercapacitors. *Prog. Nat. Sci. Mater. Int.* **2015**, *25*, 554–562.

(13) Liu, M.; Zhang, R.; Chen, W. Graphene-Supported Nanoelectrocatalysts for Fuel Cells: Synthesis, Properties, and Applications. *Chem. Rev.* **2014**, *114*, 5117–5160.

(14) Jo, G.; Choe, M.; Lee, S.; Park, W.; Kahng, Y. H.; Lee, T. The Application of Graphene as Electrodes in Electrical and Optical Devices. *Nanotechnology* **2012**, *23*, 112001.

(15) Liu, J.; Xue, Y.; Dai, L. Sulfated Graphene Oxide as a Hole-Extraction Layer in High-Performance Polymer Solar Cells. *J. Phys. Chem. Lett.* **2012**, *3*, 1928–1933.

(16) Lyu, C.-K.; Zheng, F.; Babu, B. H.; Niu, M.-S.; Feng, L.; Yang, J.-L.; Qin, W.; Hao, X.-T. Functionalized Graphene Oxide Enables a High-Performance Bulk Heterojunction Organic Solar Cell with a Thick Active Layer. *J. Phys. Chem. Lett.* **2018**, *9*, 6238–6248.

(17) Qi, X.; Mao, J. Current Collector-Free Reduced Graphene Oxide Aerogel Cathode for High Energy Density Dual-Ion Batteries. *J. Phys. Chem. Lett.* **2021**, *12*, 5430–5435.

(18) Bonaccorso, F.; Sun, Z.; Hasan, T.; Ferrari, A. C. Graphene Photonics and Optoelectronics. *Nat. Photonics* **2010**, *4*, 611–622.

(19) He, Q.; Wu, S.; Gao, S.; Cao, X.; Yin, Z.; Li, H.; Chen, P.; Zhang, H. Transparent, Flexible, All-Reduced Graphene Oxide Thin Film Transistors. *ACS Nano* **2011**, *5*, 5038–5044.

(20) Murray, I. P.; Lou, S. J.; Cote, L. J.; Loser, S.; Kadleck, C. J.; Xu, T.; Szarko, J. M.; Rolczynski, B. S.; Johns, J. E.; Huang, J.; *et al.* Graphene Oxide Interlayers for Robust, High-Efficiency Organic Photovoltaics. *J. Phys. Chem. Lett.* **2011**, *2*, 3006–3012.

(21) Avouris, P.; Xia, F. Graphene Applications in Electronics and Photonics. *MRS Bull.* **2012**, *37*, 1225–1234.

(22) Zhou, M.; Zhai, Y.; Dong, S. Electrochemical Sensing and Biosensing Platform Based on Chemically Reduced Graphene Oxide. *Anal. Chem.* **2009**, *81*, 5603–5613.

(23) Fan, Z.; Kanchanapally, R.; Ray, P. C. Hybrid Graphene Oxide Based Ultrasensitive SERS Probe for Label-Free Biosensing. *J. Phys. Chem. Lett.* **2013**, *4*, 3813–3818.

(24) Tissera, N. D.; Wijesena, R. N.; Perera, J. R.; De Silva, K. M. N.; Amaratunge, G. A. J. Hydrophobic Cotton Textile Surfaces Using an Amphiphilic Graphene Oxide (GO) Coating. *Appl. Surf. Sci.* **2015**, *324*, 455–463.

(25) Bao, Q.; Zhang, D.; Qi, P. Synthesis and Characterization of Silver Nanoparticle and Graphene Oxide Nanosheet Composites as a Bactericidal Agent for Water Disinfection. *J. Colloid Interface Sci.* **2011**, *360*, 463–470.

(26) Abdelhalim, A. O. E.; Galal, A.; Hussein, M. Z.; El Sayed, I. E. T. Graphene Functionalization by 1,6-Diaminohexane and Silver Nanoparticles for Water Disinfection. *J. Nanomater.* **2016**, *2016*, 1485280.

(27) Fan, Z.; Yust, B.; Nellore, B. P. V.; Sinha, S. S.; Kanchanapally, R.; Crouch, R. A.; Pramanik, A.; Chavva, S. R.; Sardar, D.; Ray, P. C. Accurate Identification and Selective Removal of Rotavirus Using a Plasmonic–Magnetic 3D Graphene Oxide Architecture. *J.*

Phys. Chem. Lett. **2014**, *5*, 3216–3221.

(28)   Hegab, H. M.; Zou, L. Graphene Oxide-Assisted Membranes: Fabrication and Potential Applications in Desalination and Water Purification. *J. Memb. Sci.* **2015**, *484*, 95–106.

(29)   Raffone, F.; Savazzi, F.; Cicero, G. Controlled Pore Generation in Single-Layer Graphene Oxide for Membrane Desalination. *J. Phys. Chem. Lett.* **2019**, *10*, 7492–7497.

(30)   Yang, X.; Zhang, X.; Ma, Y.; Huang, Y.; Wang, Y.; Chen, Y. Superparamagnetic Graphene Oxide-Fe3O4 Nanoparticles Hybrid for Controlled Targeted Drug Carriers. *J. Mater. Chem.* **2009**, *19*, 2710–2714.

(31)   Liu, J.; Cui, L.; Losic, D. Graphene and Graphene Oxide as New Nanocarriers for Drug Delivery Applications. *Acta Biomater.* **2013**, *9*, 9243–9257.

(32)   Mousavi, S. M.; Hashemi, S. A.; Ghasemi, Y.; Amani, A. M.; Babapoor, A.; Arjmand, O. Applications of Graphene Oxide in Case of Nanomedicines and Nanocarriers for Biomolecules: Review Study. *Drug Metab. Rev.* **2019**, *51*, 12–41.

(33)   Kim, H.; Namgung, R.; Singha, K.; Oh, I. K.; Kim, W. J. Graphene Oxide-Polyethylenimine Nanoconstruct as a Gene Delivery Vector and Bioimaging Tool. *Bioconjug. Chem.* **2011**, *22*, 2558–2567.

(34)   Liu, B.; Salgado, S.; Maheshwari, V.; Liu, J. DNA Adsorbed on Graphene and Graphene Oxide: Fundamental Interactions, Desorption and Applications. *Curr. Opin. Colloid Interface Sci.* **2016**, *26*, 41–49.

(35)   Shen, J.; Shi, M.; Yan, B.; Ma, H.; Li, N.; Hu, Y.; Ye, M. Covalent Attaching Protein to Graphene Oxide *via* Diimide-Activated Amidation. *Colloids Surfaces B Biointerfaces* **2010**, *81*, 434–438.

(36)   Zhang, X.; Niu, J.; Zhang, X.; Xiao, R.; Lu, M.; Cai, Z. Graphene Oxide-SiO$_2$

Nanocomposite as the Adsorbent for Extraction and Preconcentration of Plant Hormones for HPLC Analysis. *J. Chromatogr. B Anal. Technol. Biomed. Life Sci.* **2017**, *1046*, 58–64.

(37) Li, Y.; Lu, Q.; Liu, H.; Wang, J.; Zhang, P.; Liang, H.; Jiang, L.; Wang, S. Antibody-Modified Reduced Graphene Oxide Films with Extreme Sensitivity to Circulating Tumor Cells. *Adv. Mater.* **2015**, *27*, 6848–6854.

(38) Lin, H.; Liu, Y.; Huo, J.; Zhang, A.; Pan, Y.; Bai, H.; Jiao, Z.; Fang, T.; Wang, X.; Cai, Y.; *et al.* Modified Enzyme-Linked Immunosorbent Assay Strategy Using Graphene Oxide Sheets and Gold Nanoparticles Functionalized with Different Antibody Types. *Anal. Chem.* **2013**, *85*, 6228–6232.

(39) Shin, S. R.; Zihlmann, C.; Akbari, M.; Assawes, P.; Cheung, L.; Zhang, K.; Manoharan, V.; Zhang, Y. S.; Yüksekkaya, M.; Wan, K. T.; *et al.* Reduced Graphene Oxide-GelMA Hybrid Hydrogels as Scaffolds for Cardiac Tissue Engineering. *Small* **2016**, *12*, 3677–3689.

(40) Wang, Z.; Huang, P.; Bhirde, A.; Jin, A.; Ma, Y.; Niu, G.; Neamati, N.; Chen, X. A Nanoscale Graphene Oxide–Peptide Biosensor for Real-Time Specific Biomarker Detection on the Cell Surface. *Chem. Commun.* **2012**, *48*, 9768–9770.

(41) Feng, L.; Wu, L.; Qu, X. New Horizons for Diagnostics and Therapeutic Applications of Graphene and Graphene Oxide. *Adv. Mater.* **2013**, *25*, 168–186.

(42) Shen, A. J.; Li, D. L.; Cai, X. J.; Dong, C. Y.; Dong, H. Q.; Wen, H. Y.; Dai, G. H.; Wang, P. J.; Li, Y. Y. Multifunctional Nanocomposite Based on Graphene Oxide for *in Vitro* Hepatocarcinoma Diagnosis and Treatment. *J. Biomed. Mater. Res. - Part A* **2012**, *100 A*, 2499–2506.

(43) Zang, Z.; Zeng, X.; Wang, M.; Hu, W.; Liu, C.; Tang, X. Tunable Photoluminescence of Water-Soluble AgInZnS–Graphene Oxide (GO) Nanocomposites and Their Application in-

Vivo Bioimaging. *Sensors Actuators, B Chem.* **2017**, *252*, 1179–1186.

(44) Zhu, S.; Zhang, J.; Qiao, C.; Tang, S.; Li, Y.; Yuan, W.; Li, B.; Tian, L.; Liu, F.; Hu, R.; *et al.* Strongly Green-Photoluminescent Graphene Quantum Dots for Bioimaging Applications. *Chem. Commun.* **2011**, *47*, 6858–6860.

(45) Kundu, N.; Mukherjee, D.; Maiti, T. K.; Sarkar, N. Protein-Guided Formation of Silver Nanoclusters and Their Assembly with Graphene Oxide as an Improved Bioimaging Agent with Reduced Toxicity. *J. Phys. Chem. Lett.* **2017**, *8*, 2291–2297.

(46) Pramanik, A.; Chavva, S. R.; Fan, Z.; Sinha, S. S.; Nellore, B. P. V.; Ray, P. C. Extremely High Two-Photon Absorbing Graphene Oxide for Imaging of Tumor Cells in the Second Biological Window. *J. Phys. Chem. Lett.* **2014**, *5*, 2150–2154.

(47) Bolibok, P.; Roszek, K.; Wiśniewski, M. Graphene Oxide-Mediated Protection from Photodamage. *J. Phys. Chem. Lett.* **2018**, *9*, 3241–3244.

(48) Ye, S.; Shao, K.; Li, Z.; Guo, N.; Zuo, Y.; Li, Q.; Lu, Z.; Chen, L.; He, Q.; Han, H. Antiviral Activity of Graphene Oxide: How Sharp Edged Structure and Charge Matter. *ACS Appl. Mater. Interfaces* **2015**, *7*, 21578–21579.

(49) Liu, S.; Zeng, T. H.; Hofmann, M.; Burcombe, E.; Wei, J.; Jiang, R.; Kong, J.; Chen, Y. Antibacterial Activity of Graphite, Graphite Oxide, Graphene Oxide, and Reduced Graphene Oxide: Membrane and Oxidative Stress. *ACS Nano* **2011**, *5*, 6971–6980.

(50) Chen, J.; Peng, H.; Wang, X.; Shao, F.; Yuan, Z.; Han, H. Graphene Oxide Exhibits Broad-Spectrum Antimicrobial Activity against Bacterial Phytopathogens and Fungal Conidia by Intertwining and Membrane Perturbation. *Nanoscale* **2014**, *6*, 1879–1889.

(51) Zhang, L.; Xia, J.; Zhao, Q.; Liu, L.; Zhang, Z. Functional Graphene Oxide as a Nanocarrier for Controlled Loading and Targeted Delivery of Mixed Anticancer Drugs. *Small* **2010**, *6*,

537–544.

(52) Yang, X.; Wang, Y.; Huang, X.; Ma, Y.; Huang, Y.; Yang, R.; Duan, H.; Chen, Y. Multi-Functionalized Graphene Oxide Based Anticancer Drug-Carrier with Dual-Targeting Function and pH-Sensitivity. *J. Mater. Chem.* **2011**, *21*, 3448–3454.

(53) Gurunathan, S.; Han, J. W.; Park, J.-H.; Kim, E. S.; Choi, Y.-J.; Kwon, D.-N.; Kim, J.-H. Reduced Graphene Oxide&Ndash;Silver Nanoparticle Nanocomposite: A Potential Anticancer Nanotherapy. *Int. J. Nanomedicine* **2015**, *10*, 6257.

(54) Geim, A. K.; Novoselov, K. S. The Rise of Graphene. *Nat. Mater.* **2007**, *6*, 183–191.

(55) Huang, L.; Chang, Q. H.; Guo, G. L.; Liu, Y.; Xie, Y. Q.; Wang, T.; Ling, B.; Yang, H. F. Synthesis of High-Quality Graphene Films on Nickel Foils by Rapid Thermal Chemical Vapor Deposition. *Carbon N. Y.* **2012**, *50*, 551–556.

(56) Zhou, M.; Tang, J.; Cheng, Q.; Xu, G.; Cui, P.; Qin, L. C. Few-Layer Graphene Obtained by Electrochemical Exfoliation of Graphite Cathode. *Chem. Phys. Lett.* **2013**, *572*, 61–65.

(57) Chang, Y. M.; Kim, H.; Lee, J. H.; Song, Y. W. Multilayered Graphene Efficiently Formed by Mechanical Exfoliation for Nonlinear Saturable Absorbers in Fiber Mode-Locked Lasers. *Appl. Phys. Lett.* **2010**, *97*, 211102.

(58) Chen, W.; Yan, L.; Bangal, P. R. Preparation of Graphene by the Rapid and Mild Thermal Reduction of Graphene Oxide Induced by Microwaves. *Carbon N. Y.* **2010**, *48*, 1146–1152.

(59) Chua, C. K.; Pumera, M. Chemical Reduction of Graphene Oxide: A Synthetic Chemistry Viewpoint. *Chem. Soc. Rev.* **2014**, *43*, 291–312.

(60) Shao, Y.; Wang, J.; Engelhard, M.; Wang, C.; Lin, Y. Facile and Controllable Electrochemical Reduction of Graphene Oxide and Its Applications. *J. Mater. Chem.* **2010**, *20*, 743–748.

(61)   Brodie, B. C. XIII. On the Atomic Weight of Graphite. *Philos. Trans. R. Soc. London* **1859**, *149*, 249–259.

(62)   Staudenmaier, L. Verfahren zur Darstellung der Graphitsäure. *Berichte der Dtsch. Chem. Gesellschaft* **1898**, *31*, 1481–1487.

(63)   Hofmann, U.; König, E. Untersuchungen über Graphitoxyd. *Zeitschrift für Anorg. und Allg. Chemie* **1937**, *234*, 311–336.

(64)   Hummers, W. S.; Offeman, R. E. Preparation of Graphitic Oxide. *J. Am. Chem. Soc.* **1958**, *80*, 1339.

(65)   Marcano, D. C.; Kosynkin, D. V.; Berlin, J. M.; Sinitskii, A.; Sun, Z.; Slesarev, A.; Alemany, L. B.; Lu, W.; Tour, J. M. Improved Synthesis of Graphene Oxide. *ACS Nano* **2010**, *4*, 4806–4814.

(66)   Feicht, P.; Biskupek, J.; Gorelik, T. E.; Renner, J.; Halbig, C. E.; Maranska, M.; Puchtler, F.; Kaiser, U.; Eigler, S. Brodie's or Hummers' Method: Oxidation Conditions Determine the Structure of Graphene Oxide. *Chem. - A Eur. J.* **2019**, *25*, 8955–8959.

(67)   Chaban, V. V.; Fileti, E. E.; Prezhdo, O. V. Buckybomb: Reactive Molecular Dynamics Simulation. *J. Phys. Chem. Lett.* **2015**, *6*, 913–917.

(68)   Chaban, V. V.; Prezhdo, O. V. Haber Process Made Efficient by Hydroxylated Graphene: *Ab Initio* Thermochemistry and Reactive Molecular Dynamics. *J. Phys. Chem. Lett.* **2016**, *7*, 2622–2626.

(69)   Suk, M. E.; Aluru, N. R. Water Transport through Ultrathin Graphene. *J. Phys. Chem. Lett.* **2010**, *1*, 1590–1594.

(70)   Meng, F.; Chen, C.; Song, J. Dislocation Shielding of a Nanocrack in Graphene: Atomistic Simulations and Continuum Modeling. *J. Phys. Chem. Lett.* **2015**, *6*, 4038–4042.

(71) Haar, S.; Bruna, M.; Lian, J. X.; Tomarchio, F.; Olivier, Y.; Mazzaro, R.; Morandi, V.; Moran, J.; Ferrari, A. C.; Beljonne, D.; *et al.* Liquid-Phase Exfoliation of Graphite into Single- and Few-Layer Graphene with α-Functionalized Alkanes. *J. Phys. Chem. Lett.* **2016**, *7*, 2714–2721.

(72) Zhu, Q.; Lu, Y. H.; Jiang, J. Z. Stability and Properties of Two-Dimensional Graphene Hydroxide. *J. Phys. Chem. Lett.* **2011**, *2*, 1310–1314.

(73) Strong, S. E.; Eaves, J. D. Atomistic Hydrodynamics and the Dynamical Hydrophobic Effect in Porous Graphene. *J. Phys. Chem. Lett.* **2016**, *7*, 1907–1912.

(74) Al-Muhit, B.; Sanchez, F. Tunable Mechanical Properties of Graphene by Clustered Line Pattern Hydroxyl Functionalization *via* Molecular Dynamics Simulations. *Carbon N. Y.* **2019**, *146*, 680–700.

(75) Tang, H.; Liu, D.; Zhao, Y.; Yang, X.; Lu, J.; Cui, F. Molecular Dynamics Study of the Aggregation Process of Graphene Oxide in Water. *J. Phys. Chem. C* **2015**, *119*, 26712–26718.

(76) Bagri, A.; Mattevi, C.; Acik, M.; Chabal, Y. J.; Chhowalla, M.; Shenoy, V. B. Structural Evolution during the Reduction of Chemically Derived Graphene Oxide. *Nat. Chem. 2010 27* **2010**, *2*, 581–587.

(77) Neto, A. J. P.; Chaban, V. V.; Fileti, E. E. Hydration Peculiarities of Graphene Oxides with Multiple Oxidation Degrees. *Phys. Chem. Chem. Phys.* **2017**, *19*, 32333–32340.

(78) Medhekar, N. V.; Ramasubramaniam, A.; Ruoff, R. S.; Shenoy, V. B. Hydrogen Bond Networks in Graphene Oxide Composite Paper: Structure and Mechanical Properties. *ACS Nano* **2010**, *4*, 2300–2306.

(79) Shih, C.-J.; Lin, S.; Sharma, R.; Strano, M. S.; Blankschtein, D. Understanding the PH-

Dependent Behavior of Graphene Oxide Aqueous Solutions: A Comparative Experimental and Molecular Dynamics Simulation Study. *Langmuir* **2012**, *28*, 235–241.

(80) Das, T. K.; Banerjee, S.; Pandey, M.; Vishwanadh, B.; Kshirsagar, R. J.; Sudarsan, V. Effect of Surface Functional Groups on Hydrogen Adsorption Properties of Pd Dispersed Reduced Graphene Oxide. *Int. J. Hydrogen Energy* **2017**, *42*, 8032–8041.

(81) Vieira, M. A.; Gonçalves, G. R.; Cipriano, D. F.; Schettino, M. A.; Silva Filho, E. A.; Cunha, A. G.; Emmerich, F. G.; Freitas, J. C. C. Synthesis of Graphite Oxide from Milled Graphite Studied by Solid-State 13C Nuclear Magnetic Resonance. *Carbon N. Y.* **2016**, *98*, 496–503.

(82) Gao, W.; Alemany, L. B.; Ci, L.; Ajayan, P. M. New Insights into the Structure and Reduction of Graphite Oxide. *Nat. Chem.* **2009**, *1*, 403–408.

(83) Xu, G.; Malmström, J.; Edmonds, N.; Broderick, N.; Travas-Sejdic, J.; Jin, J. Investigation of the Reduction of Graphene Oxide by Lithium Triethylborohydride. *J. Nanomater.* **2016**, *2016*, 1–10.

(84) Gao, W.; Wu, G.; Janicke, M. T.; Cullen, D. A.; Mukundan, R.; Baldwin, J. K.; Brosha, E. L.; Galande, C.; Ajayan, P. M.; More, K. L.; *et al.* Ozonated Graphene Oxide Film as a Proton-Exchange Membrane. *Angew. Chemie Int. Ed.* **2014**, *53*, 3588–3593.

(85) Ossonon, B. D.; Bélanger, D. Synthesis and Characterization of Sulfophenyl-Functionalized Reduced Graphene Oxide Sheets. *RSC Adv.* **2017**, *7*, 27224–27234.

(86) Khanra, P.; Uddin, M. E.; Kim, N. H.; Kuila, T.; Lee, S. H.; Lee, J. H. Electrochemical Performance of Reduced Graphene Oxide Surface-Modified with 9-Anthracene Carboxylic Acid. *RSC Adv.* **2015**, *5*, 6443–6451.

(87) Johra, F. T.; Lee, J. W.; Jung, W. G. Facile and Safe Graphene Preparation on Solution

Based Platform. *J. Ind. Eng. Chem.* **2014**, *20*, 2883–2887.

(88) Çiplak, Z.; Yildiz, N.; Çalimli, A. Investigation of Graphene/Ag Nanocomposites Synthesis Parameters for Two Different Synthesis Methods. *Fullerenes, Nanotub. Carbon Nanostructures* **2015**, *23*, 361–370.

(89) Manchala, S.; Tandava, V. S. R. K.; Jampaiah, D.; Bhargava, S. K.; Shanker, V. Novel and Highly Efficient Strategy for the Green Synthesis of Soluble Graphene by Aqueous Polyphenol Extracts of Eucalyptus Bark and Its Applications in High-Performance Supercapacitors. *ACS Sustain. Chem. Eng.* **2019**, *7*, 11612–11620.

(90) Bose, S.; Kuila, T.; Mishra, A. K.; Kim, N. H.; Lee, J. H. Dual Role of Glycine as a Chemical Functionalizer and a Reducing Agent in the Preparation of Graphene: An Environmentally Friendly Method. *J. Mater. Chem.* **2012**, *22*, 9696.

(91) Nguyen, V. T.; Le, H. D.; Nguyen, V. C.; Tam Ngo, T. T.; Le, D. Q.; Nguyen, X. N.; Phan, N. M. Synthesis of Multi-Layer Graphene Films on Copper Tape by Atmospheric Pressure Chemical Vapor Deposition Method. *Adv. Nat. Sci. Nanosci. Nanotechnol.* **2013**, *4*, 035012.

(92) Dave, K.; Park, K. H.; Dhayal, M. Two-Step Process for Programmable Removal of Oxygen Functionalities of Graphene Oxide: Functional, Structural and Electrical Characteristics. *RSC Adv.* **2015**, *5*, 95657–95665.

(93) Rajagopalan, B.; Chung, J. S. Reduced Chemically Modified Graphene Oxide for Supercapacitor Electrode. *Nanoscale Res. Lett.* **2014**, *9*, 535.

(94) Bera, M.; Chandravati; Gupta, P.; Maji, P. K. Facile One-Pot Synthesis of Graphene Oxide by Sonication Assisted Mechanochemical Approach and Its Surface Chemistry. *J. Nanosci. Nanotechnol.* **2018**, *18*, 902–912.

(95) Sheng, Y.; Tang, X.; Peng, E.; Xue, J. Graphene Oxide Based Fluorescent Nanocomposites

for Cellular Imaging. *J. Mater. Chem. B* **2013**, *1*, 512–521.

(96)   Mohapatra, S. S.; Ranjan, S.; Dasgupta, N.; Mishra, R. K.; Thomas, S. *Characterization and Biology of Nanomaterials for Drug Delivery*; Elsevier: Oxford, UK, 2019.

(97)   Barrer, R. M.; Macleod, D. M. Intercalation and Sorption by Montmorillonite. *Trans. Faraday Soc.* **1954**, *50*, 980–989.

(98)   Chang, W. C.; Cheng, S. C.; Chiang, W. H.; Liao, J. L.; Ho, R. M.; Hsiao, T. C.; Tsai, D. H. Quantifying Surface Area of Nanosheet Graphene Oxide Colloid Using a Gas-Phase Electrostatic Approach. *Anal. Chem.* **2017**, *89*, 12217–12222.

(99)   Chen, L.; Batchelor-McAuley, C.; Rasche, B.; Johnston, C.; Hindle, N.; Compton, R. G. Surface Area Measurements of Graphene and Graphene Oxide Samples: Dopamine Adsorption as a Complement or Alternative to Methylene Blue? *Appl. Mater. Today* **2020**, *18*, 100506.

(100) Ding, S.; Sun, S.; Xu, H.; Yang, B.; Liu, Y.; Wang, H.; Chen, D.; Zhang, R. Preparation and Adsorption Property of Graphene Oxide by Using Waste Graphite from Diamond Synthesis Industry. *Mater. Chem. Phys.* **2019**, *221*, 47–57.

(101) Humphrey, W.; Dalke, A.; Schulten, K. VMD: Visual Molecular Dynamics. *J. Mol. Graph.* **1996**, *14*, 33–38.

(102) Korotkin, I.; Karabasov, S.; Nerukh, D.; Markesteijn, A.; Scukins, A.; Farafonov, V.; Pavlov, E. A Hybrid Molecular Dynamics/Fluctuating Hydrodynamics Method for Modelling Liquids at Multiple Scales in Space and Time. *J. Chem. Phys.* **2015**, *143*, 014110.

1   Table 1. The characteristics of the simulated GO stacks.

Stack number	Number of water molecules	Initial spacing, nm	Final spacing (in average), nm
#1	1478	0.75	0.92
#2	5544	1.15	1.12
#3	9539	1.5	1.46
#4	2676	1.03 (in average)	0.95
#5	1510	0.75	0.92
#6	5554	1.15	1.11
#7	9518	1.5	1.46
#8	2533	1.00 (in average)	0.94
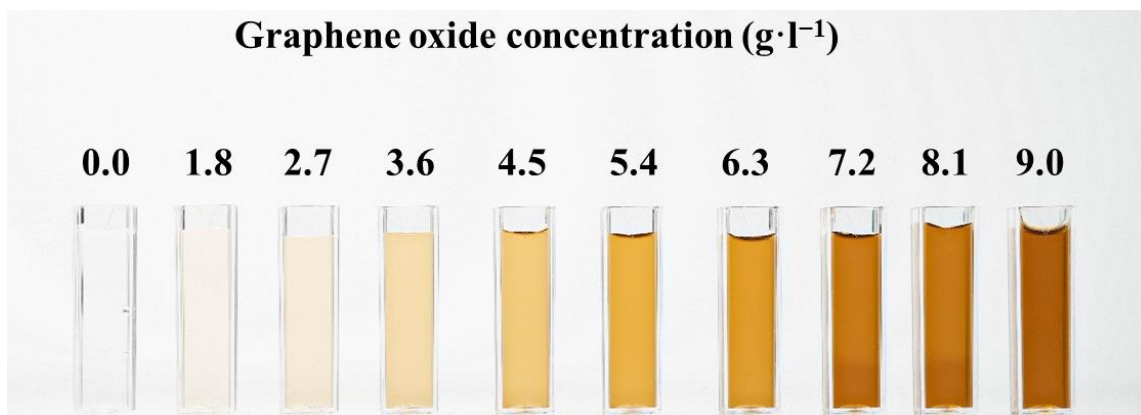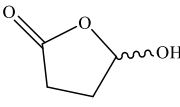
2

Fig. 1. Dispersions of GO in the concentration range $C = 1.8–9.0$ g·l^{-1}.

1
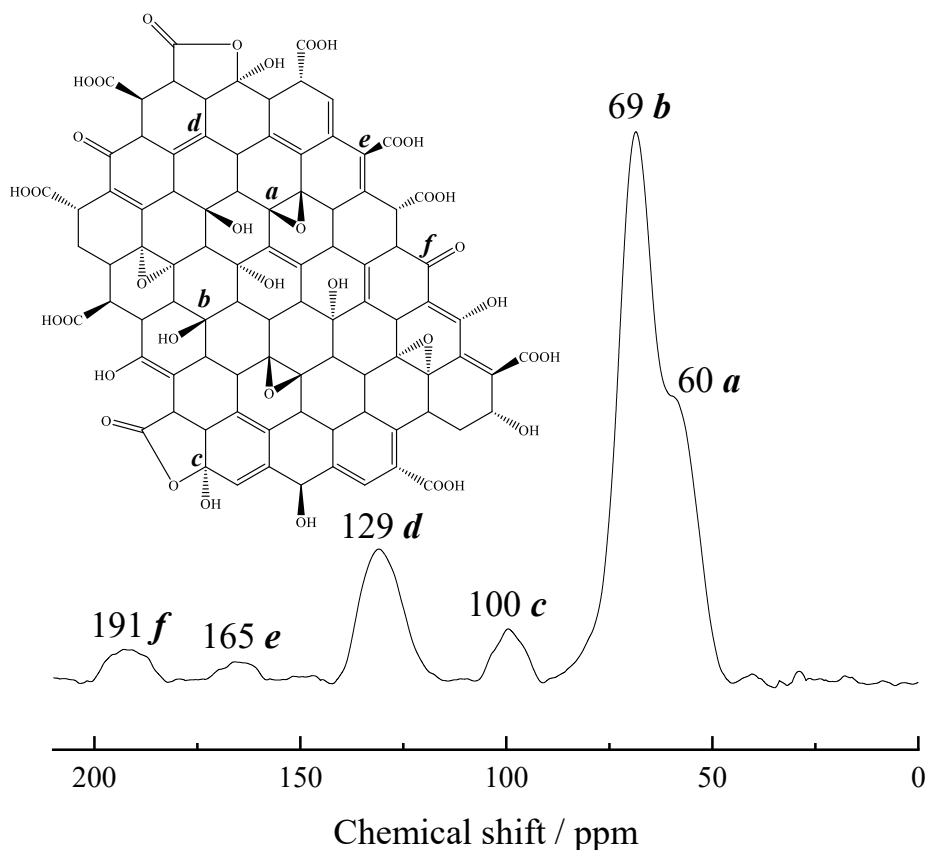
Fig. 2. ^{13}C NMR spectrum of GO obtained using direct excitation (contact time is 2 ms). *a* is a structural fragment of C–O–C located on the basal planes of the graphene sheet, *b* is a structural fragment of C–OH located on the basal planes and the edges of the graphene sheet, *c* is a structural fragment of at the edges of the graphene sheet, *d* is a structural fragment of C=C in the graphene plane, *e* is a structural fragment of –COOH at the edges of the graphene sheet, *f* is a structural fragment of C=O at the edges of the graphene sheet.

8

(*a*)
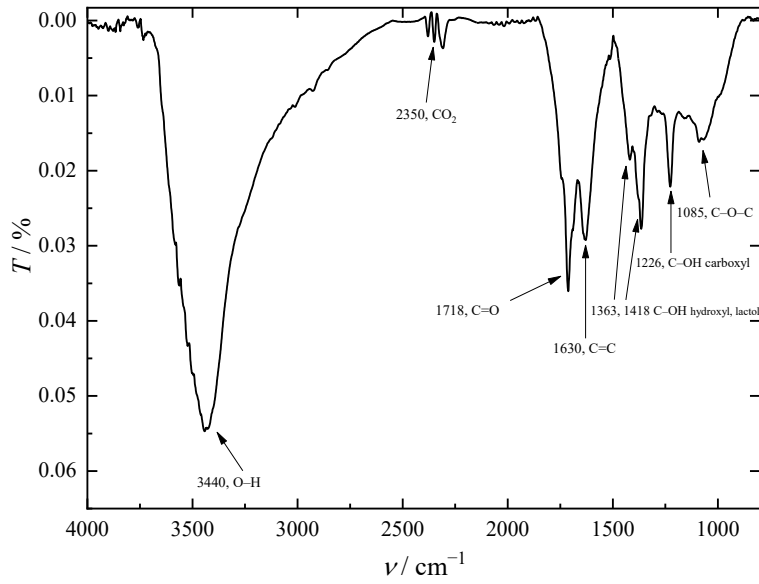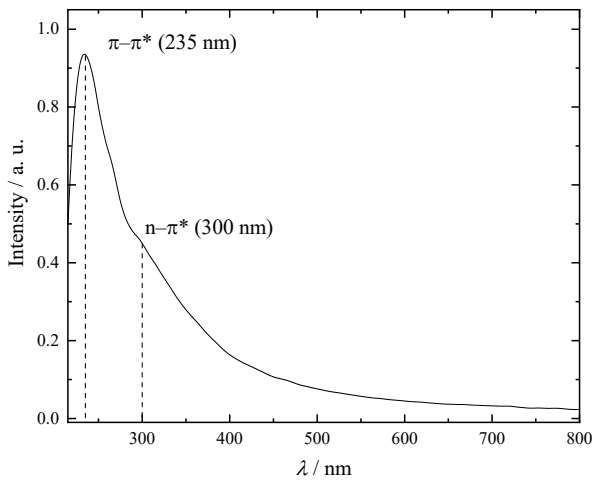
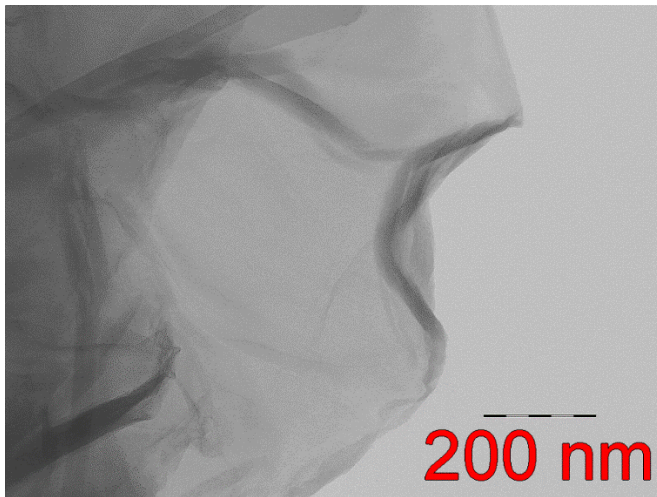(*b*)   (*c*)
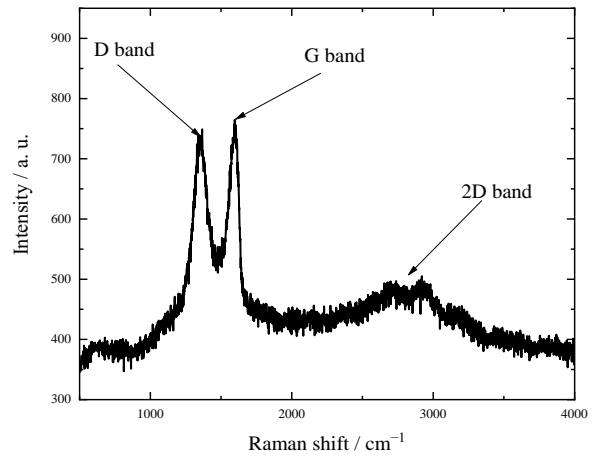
1   Fig. 3. (*a*) IR spectrum of GO; (*b*) optical excitation spectrum of GO ($C = 1.8$ g·l^{-1}); (*c*) Raman

2   spectrum of GO.

3

(*a*)

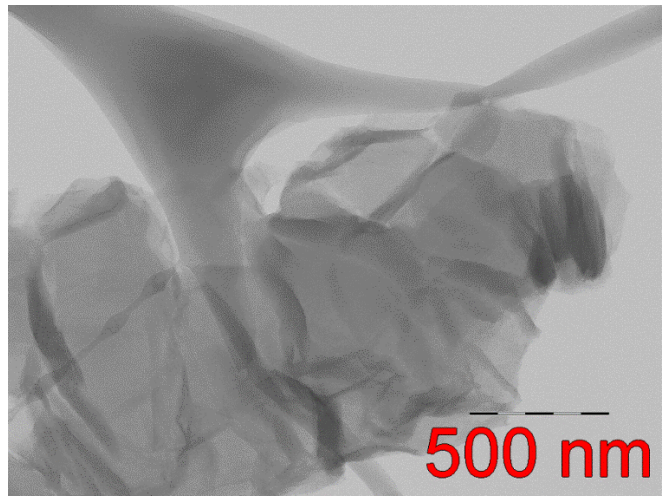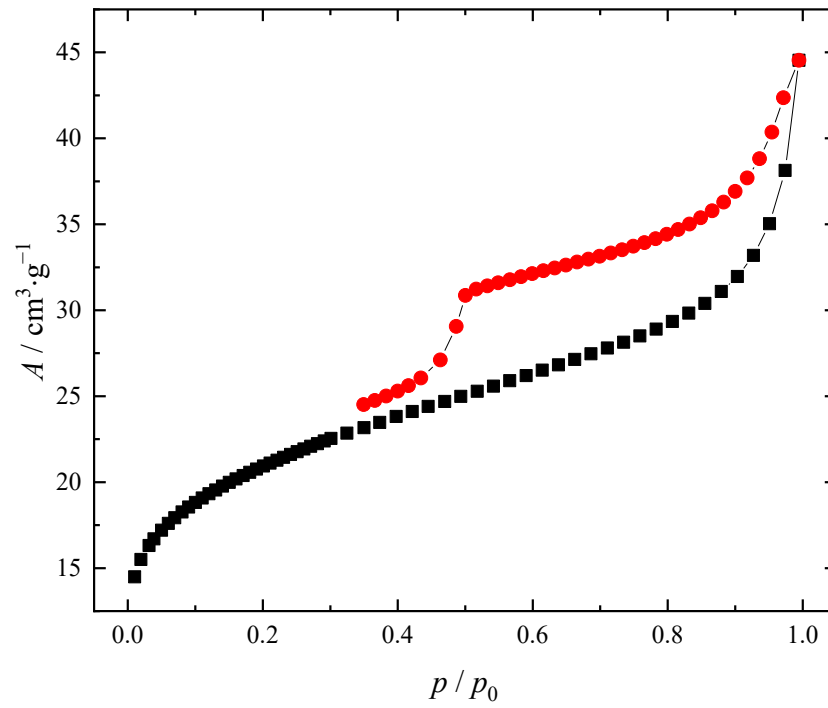(*b*)   (*c*)

200 nm

500 nm
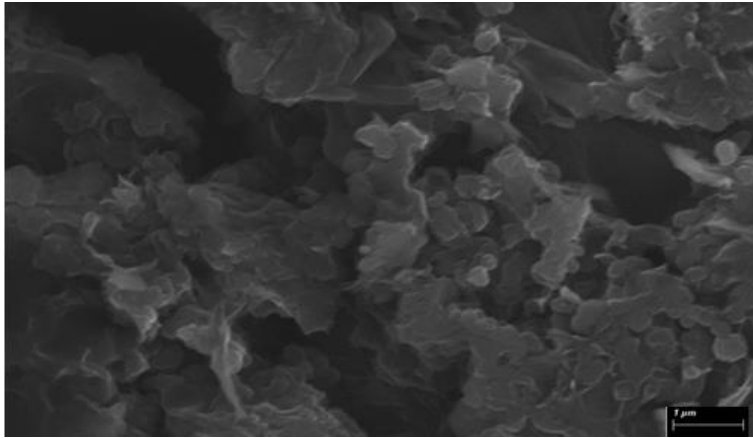
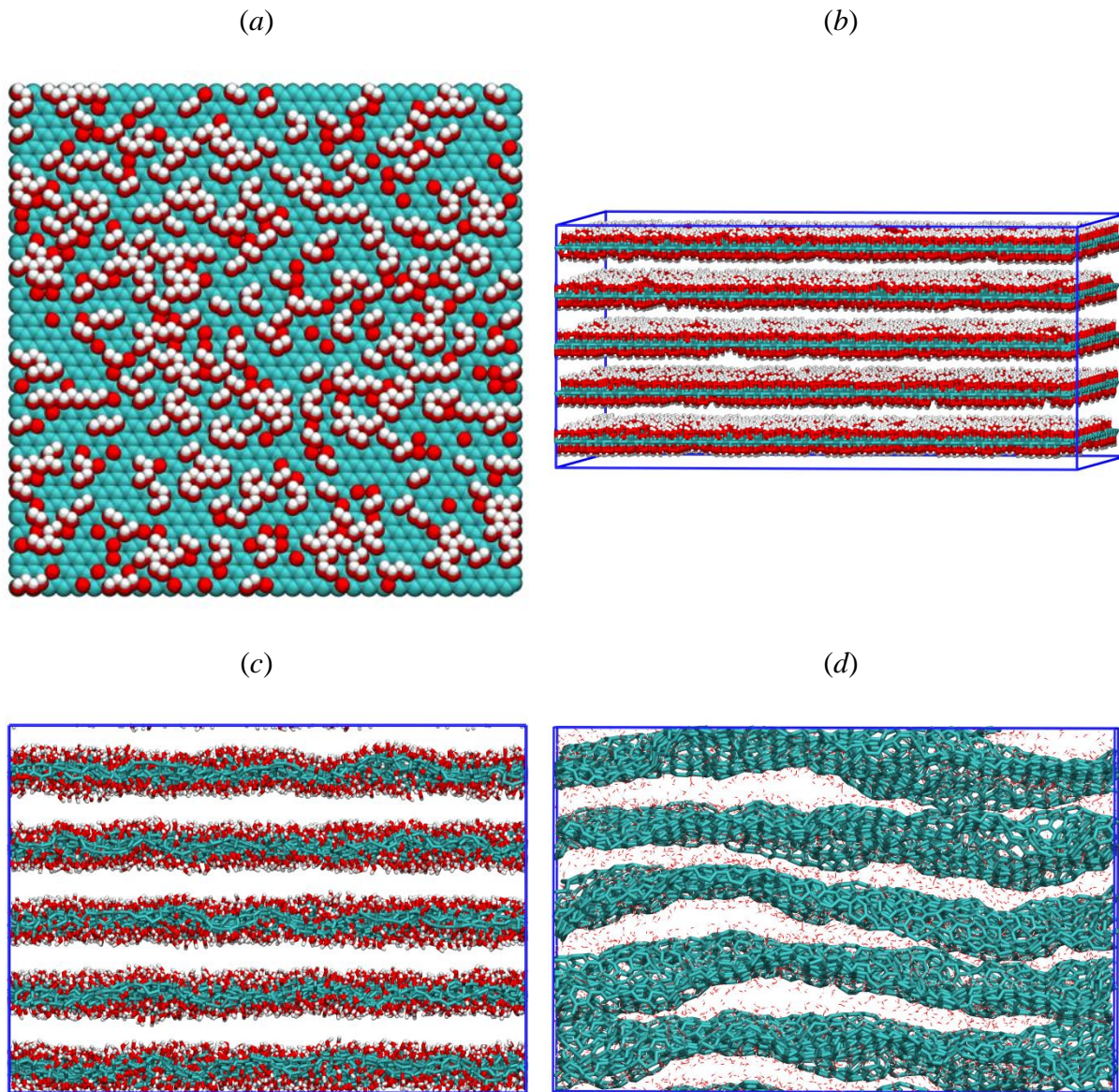1   Fig. 4. (*a*) SEM image of GO; (*b*) HRTEM image of GO.

2

1

2   Fig. 5. The nitrogen adsorption isotherm of GO at 77.4 K consisting of the adsorption branch (■)

3   and the desorption branch (●). A is the amount of the adsorbed substance, p is the gas pressure, p_0
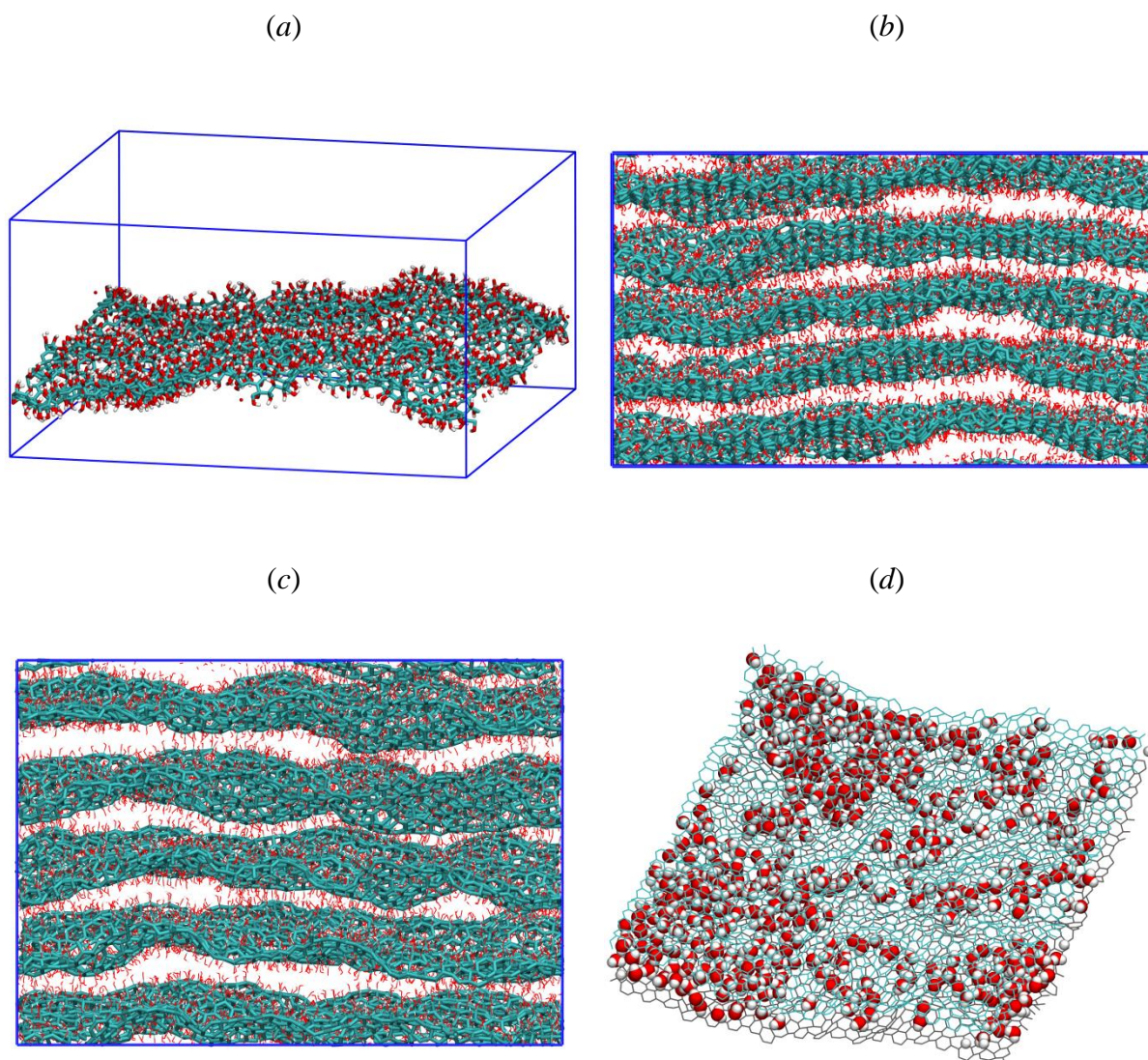
4   is the saturated vapour pressure of nitrogen.

5

Fig 6. Initial configurations of the simulated systems. Water molecules are not shown. (*a*) Single sheet before energy minimisation; (*b*) stack #1 before energy minimisation; (*c*) stack #2; (*d*) stack #4. Carbon atoms are cyan, oxygen atoms are red, hydrogen atoms are white.

(a)

(b)

(c)

(d)

Fig. 7. Final configurations of the GO sheet and stacks. (*a*) Single sheet; (*b*) stack #1; (*c*) stack #2; (*d*) water trapped between two GO sheets (coloured grey and blue, functional groups not shown) in stack #4.